J. Fluid Mech. (2021), *vol*. 916, A25, doi:10.1017/jfm.2021.215

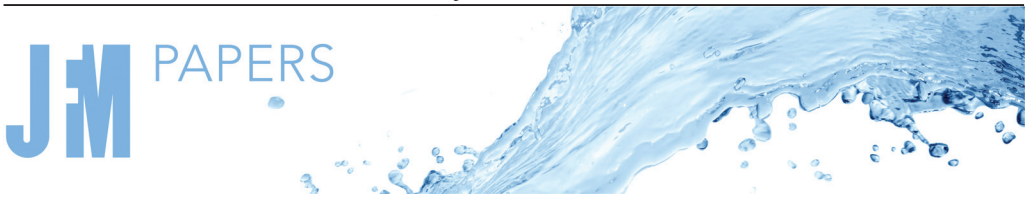

Reynolds number effect on the response of a rough wall turbulent boundary layer to local wall suction

F. Ghanadi[1],† **and L. Djenidi**[1]

[1]Mechanical Engineering, University of Newcastle, Newcastle, NSW 2308, Australia

(Received 15 September 2020; revised 28 February 2021; accepted 2 March 2021)

The combined effect of Reynolds number (Re) and localised wall suction applied through a porous strip on a fully rough wall turbulent boundary layer (TBL) is investigated using hot-wire anemometry. The measurements show that the response of the TBL to suction is modulated by the ratio U_s/U_τ, where U_s and U_τ are the suction and friction velocities, respectively. For example the suction impact on the mean velocity and the turbulence intensity profiles, which is felt across the boundary layer, decreases as U_s/U_τ decreases. Interestingly, the velocity spectra contour maps reveal that suction reduces the energy at all scales of motion across the boundary layer. Further, measurements of the velocity skewness indicate that the TBL undergoes a structural change when the ratio U_s/U_τ is relatively important. However, the measurements also reveal that TBL does not show a relaminarisation behaviour as it can be observed in a smooth wall TBL with similar localised wall suction. This lack of relaminarisation is due to the development of a growing internal boundary layer which evolves on a rough surface within the existing TBL.

Key words: turbulent boundary layers, boundary layer control

1. Introduction

In high-Reynolds-number turbulent boundary layers (TBLs), the requirement for hydrodynamic smoothness becomes unrealistically stringent due to the surface imperfections. It is thus reasonable to expect that the TBLs evolve on a hydrodynamically rough surface as the boundary layer thickness decreases with increasing Reynolds number (Re) and may reach the transitionally or fully rough regime. This raises an interesting question regarding the control of TBLs. Indeed, how a control strategy developed for a smooth wall TBL performs when the surface over which the TBL becomes hydrodynamically rough, or can a control strategy for smooth wall TBL be effective for

† Email address for correspondence: farzin.ghanadi@newcastle.edu.au

fully rough wall TBLs? Further, since a fully rough wall can become *Re*-independent (Djenidi, Talluru & Antonia 2018), is the control of fully rough wall TBL *Re*-independent? Therefore, subjecting a rough wall TBL to perturbations similar to those used to investigate the dynamic response of a smooth wall TBL is not only an academic research problem but is of great importance in many engineering applications when the aim of the flow control is to achieve particular outcomes (e.g. drag reduction, lift control and noise attenuation). It is accordingly of quite significant interest to enhance our understanding of the dynamic response of a rough wall TBL to various perturbations with increasing *Re*. To date, wall suction and injection approaches have had some success in controlling of smooth wall TBLs, particularly at low and moderate *Re* (see Gad-el Hak & Blackwelder 1989; Myose & Blackwelder 1995; Jacobson & Reynolds 1998; Park & Choi 1999; Rathnasingham & Breuer 2003; Lockerby, Carpenter & Davies 2005; Rebbeck & Choi 2006; Segawa *et al.* 2007; Kametani *et al.* 2015; Bobke, Örlü & Schlatter 2016; Qiao, Zhou & Wu 2017). Antonia *et al.* (1988) quantified the influence of wall suction, applied through a porous wall strip, on a low Reynolds number smooth wall TBL. It was found that suction could weaken the bursting process of the near-wall low-speed streaks, resulting in the reduction of turbulence energy and Reynolds stress. Antonia, Zhu & Sokolov (1995) showed that the total skin friction of a smooth wall TBL under localised wall suction via a porous strip decreases linearly with increasing suction rate. A following study (Oyewola, Djenidi & Antonia 2003) indicated that the dynamical behaviour of smooth wall TBL subjected to similar localised wall suction is *Re*-dependent. The study further demonstrated that *Re* modulates the magnitude and wavelength of the response of the TBL without changing the actual mechanism of pseudo-relaminarisation due to suction. It was also shown that with increasing *Re*, the departure of the mean velocity profiles from the corresponding undisturbed ones is less pronounced, reflecting a reduced pseudo-relaminarisation. Unfortunately, these results were obtained in smooth wall TBL where the momentum thickness-based Reynolds number (Re_θ) was less than 2000. Relaminarisation is also observed in the study conducted by Khapko *et al.* (2016), who investigated the effects of asymptotic suction on smooth TBL at low *Re* (<350). It was found that suction can remove the outer-region large eddy structures leading to development of laminar spots within the TBL which grow with the downstream distance. For a moderate Re_θ (≈ 4000), Yoshioka & Alfredsson (2006) subjected a smooth wall TBL to a uniform wall suction with a suction velocity of approximately 0.3 % of free stream velocity and observed that the turbulence production within the logarithmic region is decreased by up to 30 %. Manipulation high-*Re* wall-bounded turbulent flow using wall-normal jet has also been investigated by Marusic, Talluru & Hutchins (2014) who observed that the streamwise oriented jet can modify the large-scale structures when it actuates on the entire length of large-scale events. It was recognised that the maximum reduction in turbulence intensity occurs when the strength of the jet is correctly scaled to the strength of the detected large-scale events. When investigating the response of the outer-region of a high-*Re* TBL to external large-scale perturbations, Abbassi *et al.* (2017) showed that a large amount of the wall-normal jet-flow velocity (up to 64 % of free stream) should be synchronised with the high-speed events in order to obtain wall-shear stress reduction.

Despite the large body of work on the control of turbulent wall shear flows using wall suction garnered over the years, only a handful of studies considered the combination of wall blowing or wall suction and roughness (Healzer, Moffat & Kays 1974; Schetz & Nerney 1977; Çuhadaroğlu, Akansu & Turhal 2007; Miller, Martin & Bailey 2014; Djenidi, Kamruzzaman & Dostal 2019*a*). Miller *et al.* (2014) examined the scaling effects of combined roughness and blowing in a turbulent channel flow. The roughness consisted of a

mesh-like surface with approximately sinusoidal roughness. The surface had microcracked pores distributed uniformly over the surface that allowed mass injection through it. The authors found that the effects of roughness on the mean velocity were confined to the near-wall region, and the addition of blowing was found to be analogous to an increase in roughness effects. Further, they observed that, conversely to a smooth wall configuration, blowing increases rather than decreases the skin friction. They also observed a lack of scaling, which they associated with the blowing rate-dependent suppression of the outer-scaled large-scale motion. They also showed that the effect of blowing on the Reynolds shear stress is greatest in the near-wall region with little influence on the outer part of the boundary layer. Of particular interest, the authors indicated that, in contrast to smooth wall TBL, blowing led to an increase in the skin friction. Lately, Djenidi *et al.* (2019*a*) carried out an experimental study of a rough wall TBL subjected to localised wall suction. They found that conversely to the smooth wall case, pseudo-relaminarisation did not occur. It was argued that the inward deflection of the high-speed flow leads to strong shear layers over the surface, leading to an increase in the turbulence intensities in the vicinity of the roughness elements. The difference in the behaviour between smooth wall TBLs and rough wall TBLs subjected to wall suction stems from this fact that the dynamical behaviour of the latter TBL in the near-wall region is different from that in the former layer. In particular, the viscosity-dominated region is strongly weakened, if not entirely removed, in a rough wall TBL. There is, in fact, strong experimental evidence (Djenidi *et al.* 2018) that a fully rough wall TBLs becomes *Re*-independent, even at moderate Reynolds numbers. It in this context that it appears to be of interest to investigate whether the response of a rough wall TBL to wall suction can also become *Re*-independent. This is not possible for a smooth wall TBL. This investigation was undertaken in the present study. The study should not only provide new insights into the physics of the dynamical response of rough wall turbulent flows to perturbations over a wide range of *Re*, but also allows us to develop effective TBL control strategies in both nature and engineering applications.

The paper is organised as follows. In § 2, we briefly describe the experimental set-up and methodology. Results are presented in § 3 and the conclusion is reported in § 4.

2. Experimental procedure

The experiments are performed in an open-return blower type wind tunnel. Since the details of the facility are available in Djenidi *et al.* (2019*a*), we only present the salient features of the test section. The test section is 4 m long, with a 0.825 m wide and 0.16 m high cross-section. The tunnel has an adjustable roof which consists of two rectangular panels each of dimensions 2 m long and 0.9 m wide to allow the control of the streamwise pressure gradient. The pressure gradient is maintained at zero while the free stream velocity is changed from 5 to 35 $\mathrm{m\,s^{-1}}$. The free stream turbulence level, $\sqrt{\overline{u^2}}/U_1$, is nominally 0.5 % (at the test section located nominally 1.3 m from the inlet of the working section) for the range of free stream velocity used, where $\overline{u^2}$ is the velocity variance and U_1 is the free stream velocity. The turbulence is tripped at the entrance to the working section by a 100 mm strip of coarse grade P40 sandpaper spanning the width of the test section. Immediately downstream of the sandpaper, the boundary layer develops over a rough surface which consists of a series of cylindrical rods mounted over the entire length of the tunnel floor and spanning the entire width of the test section. The rods have a nominal diameter $k = 1.6$ mm and the distance between two consecutive rods is equal to $15k$.

U_1 (m s^{-1})	Sym.	U_s (m s^{-1})	δ (m)	δ^* (m)	$U_{\tau,p}$ (m s^{-1})	$U_s/U_{\tau,p}$	$U_{\tau,t}$ (m s^{-1})	Re_τ	θ (m)	Re_θ	l^+
		0	0.0447	0.0116	0.362	0	0.29	1079	0.0067	2050	12.1
5	◇	1.45	0.0350	0.0053	0.468	3.1		1094	0.0039	807.7	15.6
		3.3	0.0330	0.0053	0.555	5.9		1221	0.0038	800.5	18.5
		0	0.0447	0.0126	0.720	0	0.67	2147	0.0071	4617	24.1
10	□	1.45	0.0400	0.0097	0.838	1.7		2237	0.0059	3552	27.9
		3.3	0.0330	0.0081	0.955	3.4		2102	0.0054	3214	31.8
		0	0.0447	0.0124	1.078	0	0.95	3215	0.0071	6880	35.9
15	◯	1.45	0.0400	0.0108	1.196	1.2		3189	0.0064	5959	39.8
		3.3	0.0370	0.009	1.314	2.5		3214	0.0058	5400	43.8
		0	0.0531	0.0181	1.756	0	1.53	6216	0.0070	11 098	58.5
25	△	1.45	0.0531	0.0110	1.870	0.7		6620	0.0066	10 511	62.3
		3.3	0.0480	0.0096	2.010	1.6		6432	0.0060	9589	67.0
		0	0.0531	0.0116	2.525	0	2.1	8938	0.0068	15 374	84.1
35	×	1.45	0.0531	0.0011	2.661	0.5		9419	0.0066	14 623	88.7
		3.3	0.0447	0.0010	2.806	1.2		8362	0.0062	13 745	93.5

Table 1. Flow parameters for all test cases. Measurements are made at mid-distance between the second and third rods downstream of the porous strip.

Wall suction is applied locally through a porous strip of streamwise length $b = 35$ mm, spanning the full width of the test section. The strip, a sintered bronze with pore sizes in the range of 40–80 μm and mounted flush with the tunnel flow between two rods, is located 1.2 m downstream from the entrance of the working section. Two uniform suction velocities, $U_s = 1.45$ and 3.5 m s^{-1}, have been considered for the experiment. The measurements are taken at the midpoint of two consecutive roughness elements at 1.3 m from the test section inlet (between the second and third rods downstream of the porous strip) and different U_1 are used. Table 1 summarises the boundary layer characteristics for all values of U_1 (δ, δ^* and θ are the boundary layer, displacement and momentum thicknesses, respectively). The notation is as follows: the streamwise and wall-normal directions are represented by x and y, respectively, in the Cartesian system; the instantaneous and local mean streamwise velocity, are denoted by u and U, respectively; the superscript '+' indicates the scaling by inner length (ν/U_τ) and friction velocity (U_τ), where ν is kinematic viscosity. Further notation will be presented in the relevant sections.

The main challenge in rough TBL studies is associated with an accurate calculation of the friction velocity ($U_\tau = \sqrt{\tau_w/\rho}$, where τ_w is the shear stress at the wall and ρ is the air density), as many scaling laws rely on its accurate estimate (Connelly, Schultz & Flack 2006). While a number of indirect and cost-effective techniques such as cluster chart and power-law methods are available to determine U_τ over smooth surfaces, none are truly universally accepted for fully rough TBL due to the required additional parameters such as the fictitious origin for the mean velocity profile which varies with the roughness geometry. Here, the authors used the velocity defect chart method for estimating U_τ in zero pressure-gradient (ZPG) TBLs proposed by Djenidi, Talluru & Antonia (2019*b*). However, the velocity defect chart method cannot in principle be used in a non-ZPG-TBL, such in the present study, at least at the current measurement location when suction is applied.

Indeed, the present measurements are carried out near the suction where the flow experiences an inward deflection (Djenidi *et al.* 2019*a*), thus incurring a local favourable pressure gradient. For this reason, in the following we use the friction velocity, $U_{\tau,p}$, associated with the form drag measured using the pressure tap around one roughness element (full details of this method can be found in Kamruzzaman *et al.* (2014)). In table 1 we report values of both $U_{\tau,t}$ (estimated friction velocity associated with the total drag (form drag plus viscous drag)) and $U_{\tau,p}$. We observe that the latter is consistently smaller than the former, indicating that the viscous drag contribution to the total drag is negative which is consistent with the DNS results of Leonardi *et al.* (2003).

A Dantec 55P15 single hot-wire with platinum Wollaston wire is used to measure the velocity. The wire diameter (d) of 2.5 μm with an etched length (l) of 0.5 mm is soldered to the prong-tips to achieve an l/d ratio of 200, as recommended by Ligrani & Bradshaw (1987) and Hutchins *et al.* (2009). The wire is operated with an in-house constant temperature circuit at an overheat ratio of 1.5 to maintain the probe temperature at approximately 200 °C above ambient temperature. The wall-normal distance from the wall is determined using a fixed focal length microscope with a high magnification of 200 (Celestron digital microscope) mounted on a fine threaded traverse system allowing incremental steps of 1 μm. The hot-wire is mounted on a Mitutoyo height gauge, with a resolution of 0.01 m, and the velocity measurements are conducted at 32 logarithmically spaced points from 0.2 mm to 90 mm above the surface. The free stream temperature drift is monitored using a BAT-10 thermocouple, which has an accuracy of ±0.1 °C, allowing the hot-wire data to be compensated accordingly. Before and after each series of measurements of velocity profiles, the hot-wire is calibrated against a stationary Pitot-static tube located in the free stream flow at 17 different flow speeds ranging between 0 and 35 m s^{-1}. A fifth-order polynomial fit to the calibration data is used to convert the hot-wire voltages to velocities and the intermediate single point recalibration technique is used to account for calibration drift during all measurements (Talluru *et al.* 2014). The lowest frequency response of the system to an external square wave is approximately 16 kHz, occurring at zero free stream velocity, and the data are sampled at 30 kHz for 180 s. The bias error associated with the temporal resolution and sampling time is estimated to be ±2 %. We also carried out an analysis of the overall uncertainty associated with the hot-wire measurements. It was found that the estimated uncertainty derived from the experimental apparatus (i.e. data acquisition (known as DAQ) board, pressure transmitter, analogue-to-digital (known as A/D) convertor, constant temperature anemometry (CTA) system, hot-wire probe) was less than 2 %, while the uncertainty of a given measurement position is estimated to be ±0.05 mm within the measurement region.

A comment is warranted regarding the spatial resolution. As reported by Hutchins *et al.* (2009), this issue is quite pronounced in the near-wall region of the smooth TBL. They show that, when the wall normalised hot-wire length $l^+ > 40$, increasing the Reynolds number attenuates the near-wall turbulence resulting in the inability to capture correctly the peak in the streamwise velocity variance in the viscous-dominated inner region; this is in agreement with the results of Ligrani & Bradshaw (1987). Interestingly, Ligrani & Bradshaw argue that the reason for the attenuation is because length l^+ is larger than 20–25 which is larger than spanwise extends of the spanwise streak spacing (or low-speed regions), which is approximately 25. Johansson & Alfredsson (1983) also suggested that this attenuation could be attributed to spatial averaging of narrow low-speed regions. These low-speed regions are intimately linked to the mechanism of the turbulent energy at the wall. However, there is no viscous-dominated near-wall region in a fully rough wall TBL and the turbulence energy mechanism is different to that on a smooth wall (there are no

low-speed streaks in the present rough wall TBL, and the turbulent energy production is associated with the shedding of vortical structures by the rods). Further, so far there is no existing study in fully rough wall bounded turbulent flows showing or demonstrating the effects of l^+ on the statistics near the wall. It is thus not trivial to extrapolate the effects of spatial resolution on the statistics in the near-wall region of a smooth wall TBL to rough wall TBL since the dynamics of the flow in that region is entirely different between the two. While Hultmark *et al.* (2013) commented that correction accounting for spatial filtering in smooth wall TBL has not been validated for measurements in rough wall TBL, they nevertheless used it to estimate where the spatial filtering may become important over their rough wall TBL. They showed that the correction affects only the near-wall region leaving the logarithmic and wake regions practically unaffected. We performed a similar correction (not shown here) and found the effects are localised to the region $y \leq k$, which suggests that if corrections are required, they will be localised to the very near-wall region of the TBL. This observation seems to be supported by noticing that the near-wall peak in the u distributions (see the related figure) does not seem to be attenuated as the Reynolds number increases or equivalently as l^+ increases (l^+ varies from approximately 12–94), as it would if spatial resolution effects were important. It is thus reasonable to believe that for this rough wall TBL, at least in the region $y \geq k$ which is the focus of this study, the spatial resolution is good enough and quite reliable for the purpose of the present study.

3. Results

3.1. *Mean velocity*

The origin $y = 0$ for the profiles presented here is taken at the virtual origin (d_0), estimated based on the average moment per unit plan area acting on the roughness elements (see Jackson (1981) and Kamruzzaman *et al.* (2014) for further details on the method). It is found that the value of d_0 remained practically unchanged over the range of free stream and suction velocities used, $d_0 \approx 0.46k$.

Figure 1 shows distributions of the inner-normalised mean streamwise velocity, U^+, for the different suction velocities and different Re_τ ($= \delta U_{\tau,p}/\nu$) ranging from 1079 to 8362. The distributions are plotted as functions of y^+ and y/k, respectively. When no suction is applied the distributions are in agreement with the results of Djenidi *et al.* (2019*a*). There is a very good collapse of the profiles when they are plotted as function of y/k. Note that $U^+_{max} = U_1/U_{\tau,p} = [2/C_f]^{1/2}$ remains practically constant as Re_τ increases showing that C_f is constant, i.e. the form drag coefficient is Re-independent, at least when $Re_\tau > 2000$. When the profiles are plotted as functions of y^+, the profiles simply shift to higher y^+. This continuous shifting, which results from a continuous increase of U_τ with Re_τ, indicates that $\nu/U_{\tau,p}$ may not be an appropriate length scale when assessing the Re effect on the velocity field.

When suction is applied for a given U_1, the boundary layer thickness decreases and $U_{\tau,p}$ increases (see table 1). But as observed in figure 1, suction also alters the shape of the velocity profile as compared with that without suction: the larger the suction velocity, the larger the effect on the velocity profile. The effect of suction on the velocity profiles is qualitatively similar at all Reynolds number. The profile exhibits a downward shift, which reflects an increase of $U_{\tau,p}$ and intensifies with increasing U_s. However, for a given value of U_1, this downward shift reaches a limit. Indeed, for $U_s = 1.45$ and $3.5\ \mathrm{m\,s^{-1}}$ the profiles for $U_1 = 25$ and $35\ \mathrm{m\,s^{-1}}$ remain unchanged – they are practically indiscernible in the figure. This shows that the form drag coefficient recovers its Re-independent state.

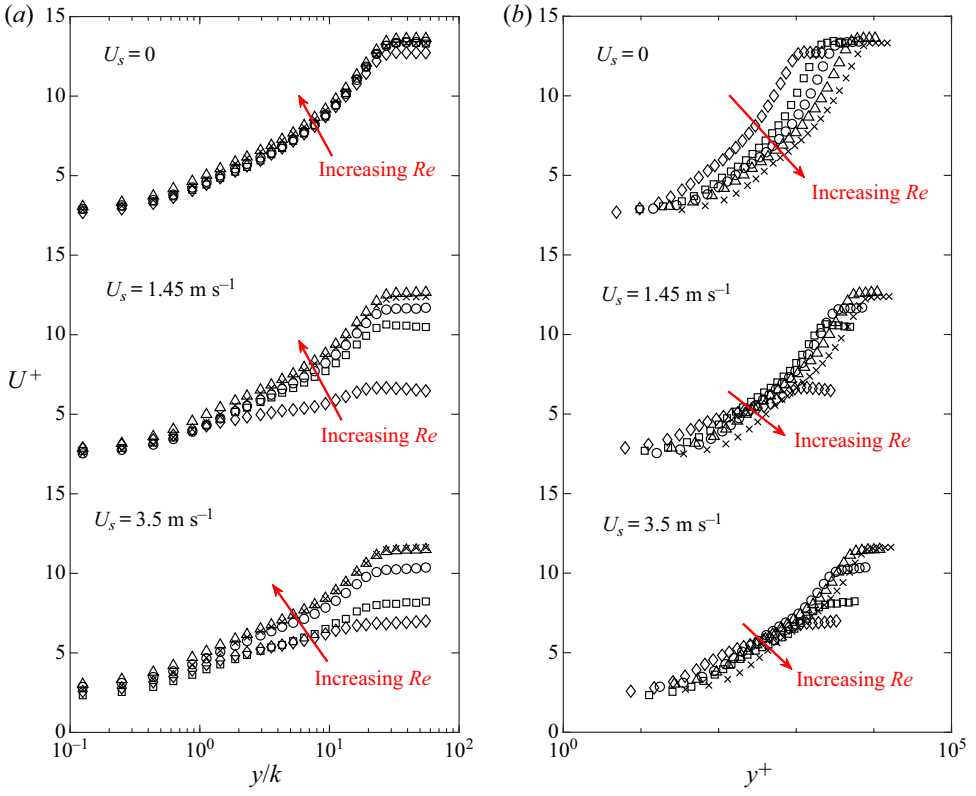

Figure 1. Inner-normalised mean streamwise velocity profiles as a function of (*a*) y/k and (*b*) y^+, at different *Re*. See table 1 for symbols.

The behaviour of the present rough wall velocity profile when suction is applied is in sharp contrast to the behaviour observed on a smooth wall under similar localised wall suction (Antonia *et al.* 1995; Oyewola *et al.* 2003). The smooth wall TBL velocity profile is observed to shift upward when suction is applied. Further, the shape of the profile approaches that of a laminar profile when relaminarisation, shown to be controlled by the suction rate and the Reynolds number, is strong. No such relaminarisation is suggested by the present velocity profiles, even at the lowest U_1 and highest U_s. Djenidi *et al.* (2019*a*) showed that just after the suction strip, the flow is subjected to a relatively strong inward deviation, where high-speed fluid from the outer region of the TBL deflects toward the wall and impacts with the roughness elements 'feeding' the process of vortex shedding taking place at the roughness element level, and thus maintaining the production of turbulent energy. Note that, an attempt at reducing Re_θ to reach the same value ($\approx$1400) as those used in Antonia *et al.* (1995) and Oyewola *et al.* (2003) and to assess whether relaminarisation in the rough wall TBL can be achieved at low Reynolds numbers was unsuccessful since that required values of U_1 to be less than approximately 3 m s^{-1}, which is too small for running the wind tunnel steadily. It is interesting to observe that, regardless of the suction velocity, the mean velocity profile exhibits a logarithmic region, although the slope and the extent of the logarithmic region decrease with increasing U_s for a given Reynolds number. The persistence of a logarithmic region as U_s increases supports the idea that relaminarisation cannot be reached on this rough wall.

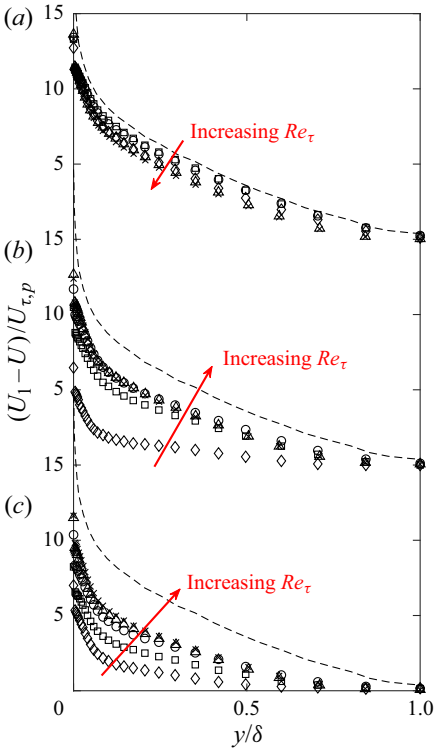

Figure 2. The mean velocity defect profiles normalised by friction velocity at different Re: (*a*) $U_s = 0$; (*b*) $U_s = 1.45\ \mathrm{m\,s^{-1}}$; (*c*) $U_s = 3.3\ \mathrm{m\,s^{-1}}$. See table 1 for symbols.

Another representation of the mean velocity profile which shows the effect of suction is seen in figure 2 where the velocity data are reported in the form of normalised velocity defect $(U_1 - U)/U_{\tau,p}$. We also report on the figure a profile (dashed line) where $U_{\tau,t}$ is used instead of $U_{\tau,p}$. That profile is representative of the universal profile onto which ZPG smooth wall and rough wall TBLs collapse (Djenidi *et al.* 2019*b*) and is used only as a reference. Notice this reference profile is shifted upward with respect to the ones when $U_{\tau,p}$ is used since $U_{\tau,t} < U_{\tau,p}$. When there is no suction, the profiles shift downward as Re_τ increases, although the profiles for two largest Re_τ collapse, indicating that the downward shift reaches a limit. When suction is applied, the profiles show a different trend as Re_τ increases: they shift upward, albeit seemingly approaching a limiting profile situated well below the reference profile; the higher the suction velocity, the larger the gap between this limiting profile and the reference one.

It should be recalled that the measurements are carried out at a downstream distance close to the suction strip. When suction is applied, the flow experiences an inward deflection where the outer high-speed fluid deviates toward the wall behind the suction strip before it recovers further downstream (Djenidi *et al.* 2019*a*). This flow deflection intensifies the shedding of vortical structures from the roughness elements, at least those strongly impacted by the inward high-velocity fluid. Further, the deflection is reflected in the reduced boundary layer thickness (see table 1), while the increase in the shedding intensity is manifested in the increase of $U_{\tau,p}$. Notice that for a given Re_τ, $U_{\tau,p}$ increases when the suction velocity increases lending credence to the idea that the vortex shedding intensifies with increasing suction.

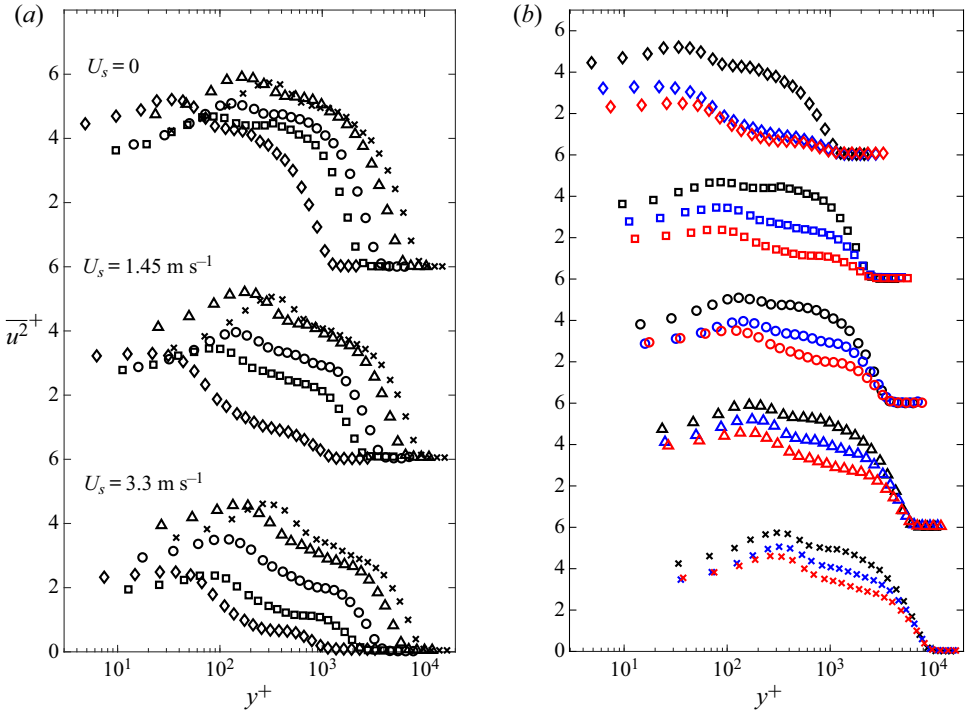

Figure 3. Distributions of the streamwise velocity variance: (*a*) *Re*-effect for a given suction velocity, (*b*) U_s-effect for a given *Re* (black, $U_s = 0$; blue, $U_s = 1.45$ m s^{-1}; red, $U_s = 3.3$ m s^{-1}). See table 1 for symbols.

3.2. *Streamwise Reynolds normal stress*

In order to better understand the dynamical response of the boundary layer to suction, the variation of the streamwise turbulence intensity across the entire boundary layer has also been investigated. We report in figure 3 the effect of suction on the distribution of $\overline{u^2}^+$ for the same cases considered in figure 1; note the upward displacement for better presentation.

Before, we carry on the analysis, some remarks are warranted regarding the distributions in the near-wall region. One can see in figure 3 that the distributions exhibit a near-wall peak, which is reminiscent of that observed in smooth wall TBL. This is in contrast with the distributions shown in Djenidi *et al.* (2018) at similar Reynolds numbers and, as here, at mid-distance between two rods. This difference can be explained by the fact that the present spacing between two rods is twice that used in Djenidi *et al.* (2018) and reflects the difference in the flow dynamics near the wall and between the rods. This was well illustrated by the numerical simulations of Leonardi *et al.* (2003). These authors show that a recirculation zone extends up to approximately $4k$ behind the first rod when the rod spacing was equal or larger than $7k$. Thus, while the measurements in Djenidi *et al.* (2018) were located at practically the reattachment point, the measurements in the present study are beyond this point.

As can be expected, and is illustrated in figure 3(*a*), suction impacts on the distribution of $\overline{u^2}^+$. For $Re_\tau = 1000$, the outer region of the initial distribution undergoes a significant change when suction is applied. However, as Re_τ increases the distribution tends to recover its original shape, although, as seen in figure 3(*a*), the magnitude of the former remains

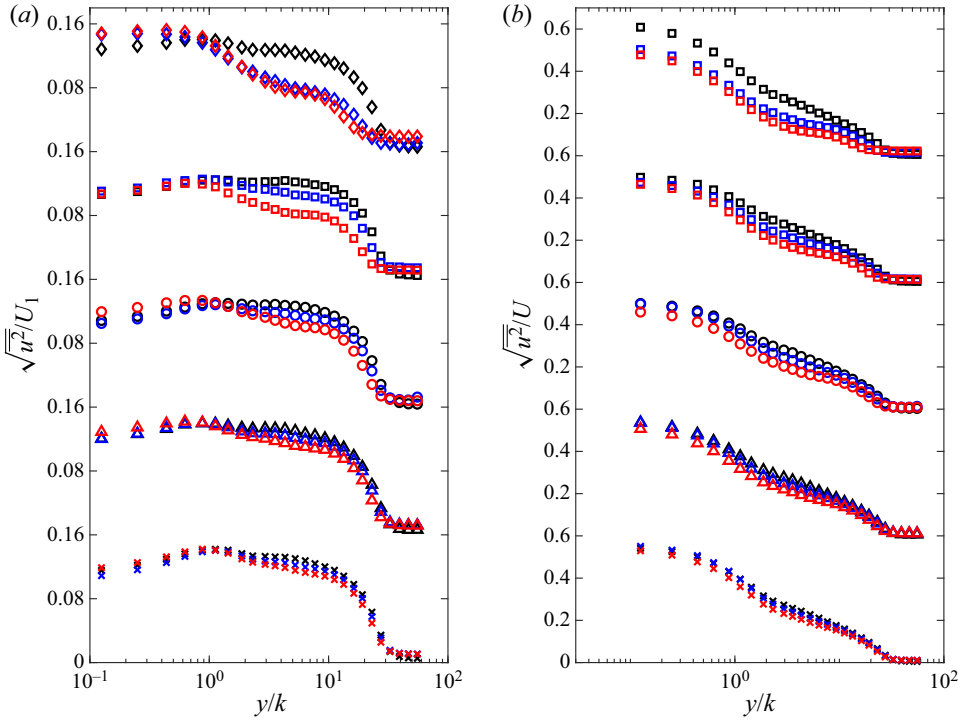

Figure 4. Effect of suction on the ratio (*a*) $\sqrt{\overline{u^2}}/U_1$ and (*b*) $\sqrt{\overline{u^2}}/U$ for different Reynolds numbers (see table 1 for symbols).

below the latter, as it should be since suction yields a larger $U_{\tau,p}$; the larger the suction velocity the larger $U_{\tau,p}$, and thus the larger the different between the perturbed and unperturbed distributions for a given Reynolds number. Of interest is the behaviour of the distributions at the lowest Re_τ. The $\overline{u^2}^+$ distributions for $U_s = 1.45$ and 3.3 m s^{-1}, respectively, collapse in the outer region (see figure 3*b*). This is consistent with the following process: a large part of the inner region of the incoming TBL is removed and replaced by a fluid with lower $\overline{u^2}^+$ deflected inward from the outer region. On the other hand, the distributions in the near-wall region deviate from each other. This deviation reduces with increasing Re_τ until it vanishes, indicating that the perturbed near-wall region becomes insensible to Re_τ, although the deviation with respect to undisturbed profile still remains.

For the present study, normalising the data by $U_{\tau,p}$ and $\nu/U_{\tau,p}$ can make the data interpretation somewhat difficult since it is observed that $U_{\tau,p}$ is impacted by suction. Therefore, we report the distributions of the ratio $(\sqrt{\overline{u^2}}/U_1)$ as a function of y/k in figure 4(*a*) for the three suction velocities at different Reynolds numbers. At low Reynolds numbers ($Re_\tau < 1300$), the data show that perturbed distributions collapse well in the region $0 \leq y/k \leq 10$, while they deviate from the unperturbed one. Also, $(\sqrt{\overline{u^2}}/U_1)$ for the perturbed TBL is larger than that for the unperturbed TBL for $y/k \leq 1$. This indicates that the turbulence activity increases in this region when suction is applied. For $1 \leq y/k \leq 10$, the perturbed TBL presents a much-reduced turbulence activity than in the unperturbed TBL. The change in the $(\sqrt{\overline{u^2}}/U_1)$ distribution is consistent with the physical mechanism

discussed above: suction deviates high-velocity fluid from the outer region towards the wall, causing some structural changes in the flow which results in a strongly altered turbulence energy distribution within the TBL. As Re_τ increases, the inward deflection of outer-layer fluid weakens as seen in the recovery of the perturbed distributions toward the unperturbed, although the perturbed distributions still deviate from the unperturbed one at the largest Re_τ, illustrating the lingering effect of suction on the TBL. This is consistent with the remark that the perturbed boundary layer does not return to its undisturbed state (Oyewola *et al.* 2003).

The results of figure 4(*a*) clearly illustrate the modulating role of the Reynolds number on the effect of suction. This modulating role is clearly seen in figure 4(*b*) which shows the ratio $(\sqrt{\overline{u^2}}/U)$. This ratio measures the importance of the velocity fluctuation u in relation to the local mean velocity U, *viz*. turbulence level. This ratio is reduced across the entire boundary layer thickness when suction is applied at low Reynolds number ($Re_\tau < 1300$), this reduction is up to 27 % near the wall. This is likely to reflect an increase in the local mean velocity, due to an intense downwash of the high-speed fluid, rather than a reduction in u. Indeed, for the same range of Re, figure 4(*a*) shows that $\sqrt{\overline{u^2}}$ increases in this near-wall region when suction is applied. As the Reynolds number increases, the ratio recovers to that of the undisturbed TBL across the boundary layer thickness. Note that the ratio $(\sqrt{\overline{u^2}}/U)$ reaches a finite non-zero value as $y/k \to 0$. The non-zero magnitude of the wall-shear stress on a smooth wall varies between 0.35 and 0.43 depending on Re ($300 < Re_\theta < 10^4$) (Oyewola *et al.* 2003; Örlü & Schlatter 2011). This is, however, less than the present value which is approximately 0.5. This shows that the turbulence level is higher in a rough wall TBL than in a smooth TBL and reflects different turbulence production mechanics between the two TBLs.

One possible rudimentary way for assessing the global effect of a control technique on the TBL would be to evaluate the following quantity:

$$\tilde{u} = \int_0^\infty \sqrt{\overline{u^2}}\,\mathrm{d}y, \tag{3.1}$$

which is simply the integral of the velocity root mean square (r.m.s.) across the boundary layer thickness. Figure 5 reports the ratio $\tilde{u}_s/\tilde{u}_{ws}$, where the subscripts s and ws represent with suction and without suction, respectively. A ratio less than one would indicate a global reduction of the turbulence intensity, which is the case for all conditions. This may not be too surprising since suction removes high turbulence intensity fluid as seen in figure 4(*a*). Note, as one may have expected, that the behaviour of this ratio is in complete correspondence with the behaviour of distributions in figure 4(*a*). Indeed, for example, the distributions for Re_τ show that $\sqrt{\overline{u^2}}/U_1$ for $U_s = 3.3\ \mathrm{m\,s^{-1}}$ is significantly below that for $U_s = 1.45\ \mathrm{m\,s^{-1}}$ across most of the boundary layer thickness and accordingly yields a smaller ratio $\tilde{u}_s/\tilde{u}_{ws}$. Also, consistent with the results of figure 4(*a*) is the effect of the Reynolds number on the suction effectiveness in reducing this ratio, which increases with the Reynolds number. Interestingly though, the ratio does not reach unity, which is consistent with the remark that the perturbed TBL does not return to its undisturbed stated. Rather, the TBL recovers an unperturbed state whose initial conditions are at the porous strip and controlled by suction. It is worth noticing that the difference in the ratios between the two suction cases is the largest at $U_1 = 10\ \mathrm{m\,s^{-1}}$. To determine whether this actually reflects a genuine dynamical response of the TBL to suction we carried out repeatability tests where the velocity measurements were repeated three times and averaged. Accounting for the systematic and measurement errors, we found that the overall uncertainty of the

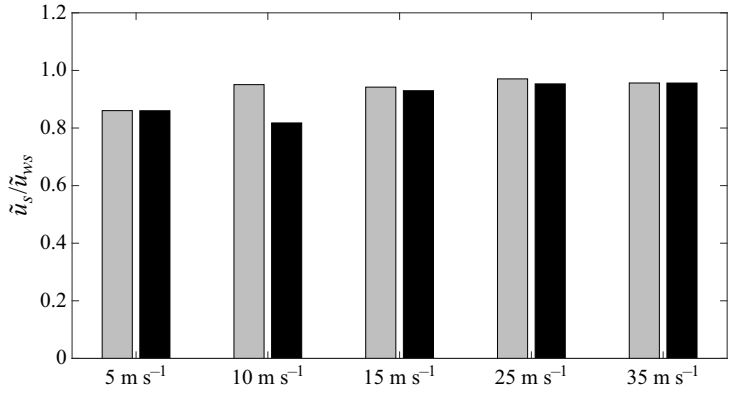

Figure 5. Ratio $\tilde{u}_s/\tilde{u}_{ws}$ for the four different values of U_1(grey bars, $U_s = 1.45\ \mathrm{m\,s^{-1}}$; black bars, $U_s = 3.3\ \mathrm{m\,s^{-1}}$).

measured mean and r.m.s. velocities was less than $\pm 2\,\%$. Therefore, the difference in the ratio between the two suction cases at $U_1 = 10\ \mathrm{m\,s^{-1}}$ is genuine as the difference falls outside the experimental uncertainty. Note that the difference in the ratio decreases as U_1 increases and practically vanishes when $U_1 = 35\ \mathrm{m\,s^{-1}}$.

The above analysis was also carried out where the normalised suction rate defined as $\sigma = (U_s b)/(U_1\theta)$, introduced by Antonia *et al.* (1995), was kept constant while changing the Reynolds number. This suction rate, also called severity index, represents the ratio of momentum flux loss due to suction and the momentum flux of the incoming boundary layer. In the present study, to maintain a constant σ while the Reynolds number, or equivalently U_1, varies one must change the suction velocity U_s accordingly. Unfortunately, it is not possible to carry out a systematic parametric analysis of the influence of Re at given σ due to the limitation imposed by the wind tunnel set-up and suction system; such study would require varying U_s from $0.3\ \mathrm{m\,s^{-1}}$ to $20\ \mathrm{m\,s^{-1}}$ for the range of Reynolds number in this work. We nevertheless were able to carry out a set of measurements with $\sigma = 0$, 0.5 and 2.5. The results are reported in figure 6. First, we observe that although σ is not relatively large, the effect of suction is nonetheless important. Second, the figure illustrates well the somewhat expected result that the higher σ for a given Reynolds number, the larger the suction effect, quantified using (3.1); in other words the effect of suction diminishes as Re increases. Third, the entire distributions are affected in term of magnitude. These results are similar to that observed in figure 3.

3.3. *Higher-order moments*

To gain further insight into the combined effect of the Reynolds number and suction on the TBL structure we now focus our attention on the third- and fourth-order statistics of the streamwise velocity. Figure 7 shows the distributions of the skewness, $S_u = \overline{u^3}/(\overline{u^2})^{3/2}$, and flatness factor, $F_u = \overline{u^4}/(\overline{u^2})^2$, for the different suction velocities and Reynolds numbers. The general shape of the distributions is similar to that of a canonical TBL (not shown here) reported in the literature. Considering that we already observed that the effects of suction are stronger at low Reynolds numbers, it is then not surprising to note that these effects on the higher-order moments are stronger at the lowest Reynolds number, while they are more pronounced for the highest velocity suction. Also, these effects are

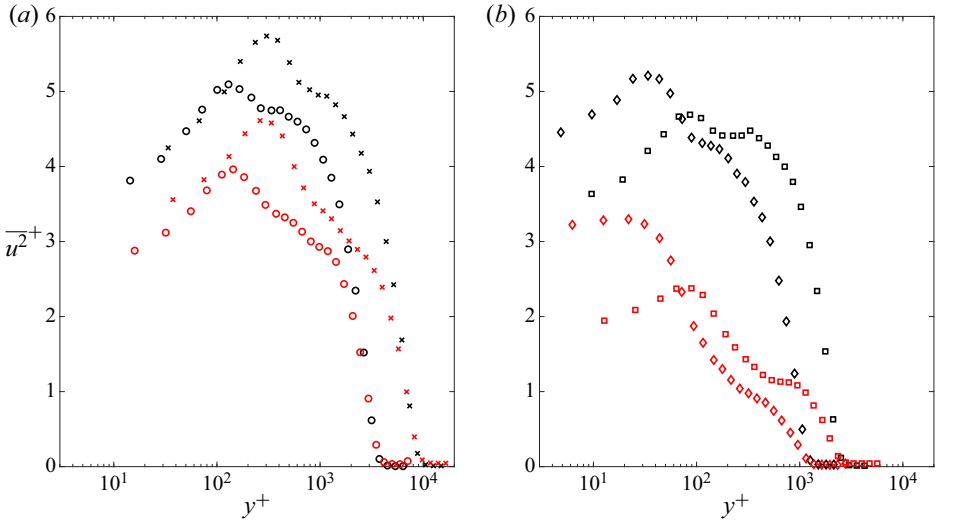

Figure 6. Combined effect of Reynolds number and σ on the streamwise velocity variance (black symbols, $\sigma = 0$; red symbols, (*a*) $\sigma = 0.5$, (*b*) $\sigma = 2.5$). See table 1 for symbols.

more noticeable on S_u than F_u, which indicates that the skewness is more sensitive to the perturbation than the flatness factor.

When suction is applied, S_u is mostly affected in the region above the roughness canopy. In this region, S_u decreases with increasing U_s. When $U_s = 0$, the values of S_u is positive, indicating that events with large negative values of $\overline{u^3}$ are not as frequent as events with large positive values of $\overline{u^3}$ (Tennekes *et al.* 1972). The situation inverses when suction is applied as indicated by the negative values of S_u, particularly for $U_s = 3.3\ \mathrm{m\,s^{-1}}$. Here, large negative values of $\overline{u^3}$ are more frequent than large positive values. This inversion process is illustrated in figure 8 which shows the probability density function (p.d.f.) of u at $y/\delta = 0.12$; this is clearly visible for the lowest Reynolds number. The undisturbed p.d.f. deviates from a Gaussian distribution with the deviation weakening as the Reynolds number increases. When suction is applied, the p.d.f. is skewed towards the positive side with its tail on the negative side being longer than that on the positive side, which is characteristic of a negative S_u. As the Reynolds number increases the perturbed p.d.f. approaches the Gaussian distribution. The behaviour of the p.d.f. when suction is applied is consistent with the description of the response of the TBL: suction deflects the TBL outer region fluid towards the wall which brings high velocity and strongly intermittent flow. This inrush of intermittent flow is also felt in the flatness factor which increases in comparison with the undisturbed case, albeit the increase may appear less pronounced than the decrease observed on S_u. As the Reynolds number increases the inward deflection weakens, thus reducing the intrusion of high-speed and strongly intermittent fluid from the outer region into the inner region, which in turn reduces the intermittency level leading to the recovery of S_u and the p.d.f.

3.4. *Spectral analysis*

While the above results provide some insight into the response of the TBL to the localised wall suction, they only inform on the global response of the TBL. Ascertaining how the perturbation may impact on the various length scales of the TBL can be achieved

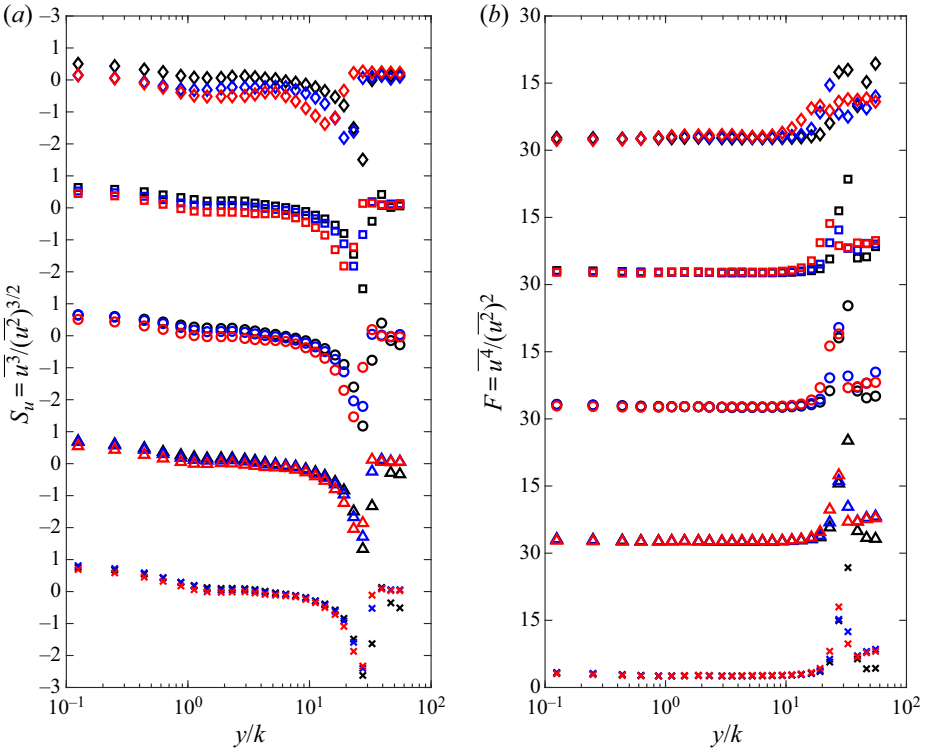

Figure 7. Distribution of (*a*) skewness, $S_u = \overline{u^3}/(\overline{u^2})^{3/2}$ and (*b*) flatness, $F_u = \overline{u^4}/(\overline{u^2})^2$ of the streamwise velocity fluctuations over a range of Re_τ. See table 1 for symbols.

in the spectral domain. We report in figure 9 the two-dimensional contour maps of the (streamwise) velocity spectra normalised by $U_{\tau,p}$ as a function of y/δ and λ_x/δ; $\lambda_x = U_c/f$ is the streamwise wavelength, which is calculated using Taylor's frozen hypothesis (Taylor 1938) where the local mean velocity U is taken as the convection velocity, U_c. This latter is critical in the application of the Taylor hypothesis and has been the subject of many investigations (see for example Squire *et al.* (2017) where the reader can find a brief literature review). Interestingly, Squire *et al.* (2017) found that, to within experimental uncertainty, the Taylor hypothesis is appropriate for the streamwise velocity component over both smooth and rough walls. However, the level of turbulence intensity measured by the ratio $\sqrt{\overline{u^2}}/U$ across their TBL was less than approximately 0.3, which is approximately the upper limit for the validity of Taylor's frozen hypothesis. In the present work and as can be seen in figure 4(*b*), the ratio $\sqrt{\overline{u^2}}/U$ exceeds 0.45 in the region $0 \leq y/k \leq 1$, indicating that the Taylor's frozen hypothesis is violated in this region; beyond that region though $\sqrt{\overline{u^2}}/U$ drops below 0.3. Considering that the Taylor hypothesis is invalid in the region $0 \leq y/k \leq 1$, we did not attempt any near-wall correction (Chung & McKeon 2010). We simply used the local velocity as the convective velocity to compute the spectra contour maps and shaded the region $0 \leq y/k \leq 1$ on those maps (see figure 9). Thus, as delimited by the vertical dashed line in the figure, the discussion will focus only on the region $y/k > 1$.

The contours shift upward when Re_τ increases for all values of U_s, revealing the growth of the wavelength λ_x of the most energetic turbulent structures with the Reynolds number.

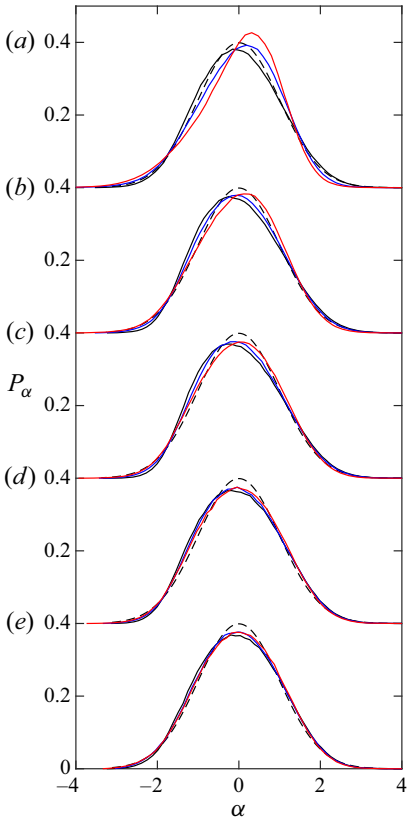

Figure 8. Probability density function of u at $y/\delta = 0.12$. Dashed line, Gaussian distribution; solid black line, $U_s = 0$; blue line, $U_s = 1.45\ \mathrm{m\,s^{-1}}$; red line, $U_s = 3.3\ \mathrm{m\,s^{-1}}$. The Re_τ is the lowest in (*a*) and highest in (*e*).

Note though that the contours for the two highest Re_τ (figure 9*d*,*e*) are practically the same suggesting that this growth saturate or at least its rate decreases with an increasing Reynolds number. Comparing the cases without and with suction one observes that suction reduces the magnitude of the contours; this effect weakens as Re_τ increases. This decrease of the spectra amplitude is consistent with the data of figure 3(*b*). Interestingly, this amplitude reduction reflects not only an increase of $U_{\tau,p}$ but also an absolute reduction in the energy, as illustrated by figure 4(*a*) where we already noted that the ratio $\sqrt{\overline{u^2}}/U_1$ in the region $y/k \geq 1$ decreases when suction is applied for all Reynolds numbers. These results show that suction reduces the energy at all scales of motion, in the region above the roughness elements.

While for the shape of the contours are practically unchanged by suction for the two highest Re_τ, they are clearly affected at the other lower Re_τ (figure 9*a–c*), particularly for large λ_x and y/δ. This is well illustrated in figure 10 where we compare the spectra contours without and with suction for the lowest and largest Reynolds numbers. For the lowest Re_τ, suction narrows the spectra contours in the region $y/\delta > 0.1$. At the highest Re_τ, the contours are barely deformed when suction is applied. These observations may suggest a structural change of the TBL at the lowest Reynolds number when suction is applied. Note that one can expect to observe such structural change at the highest Reynolds number if one increases the suction velocity U_s beyond the current maximum value.

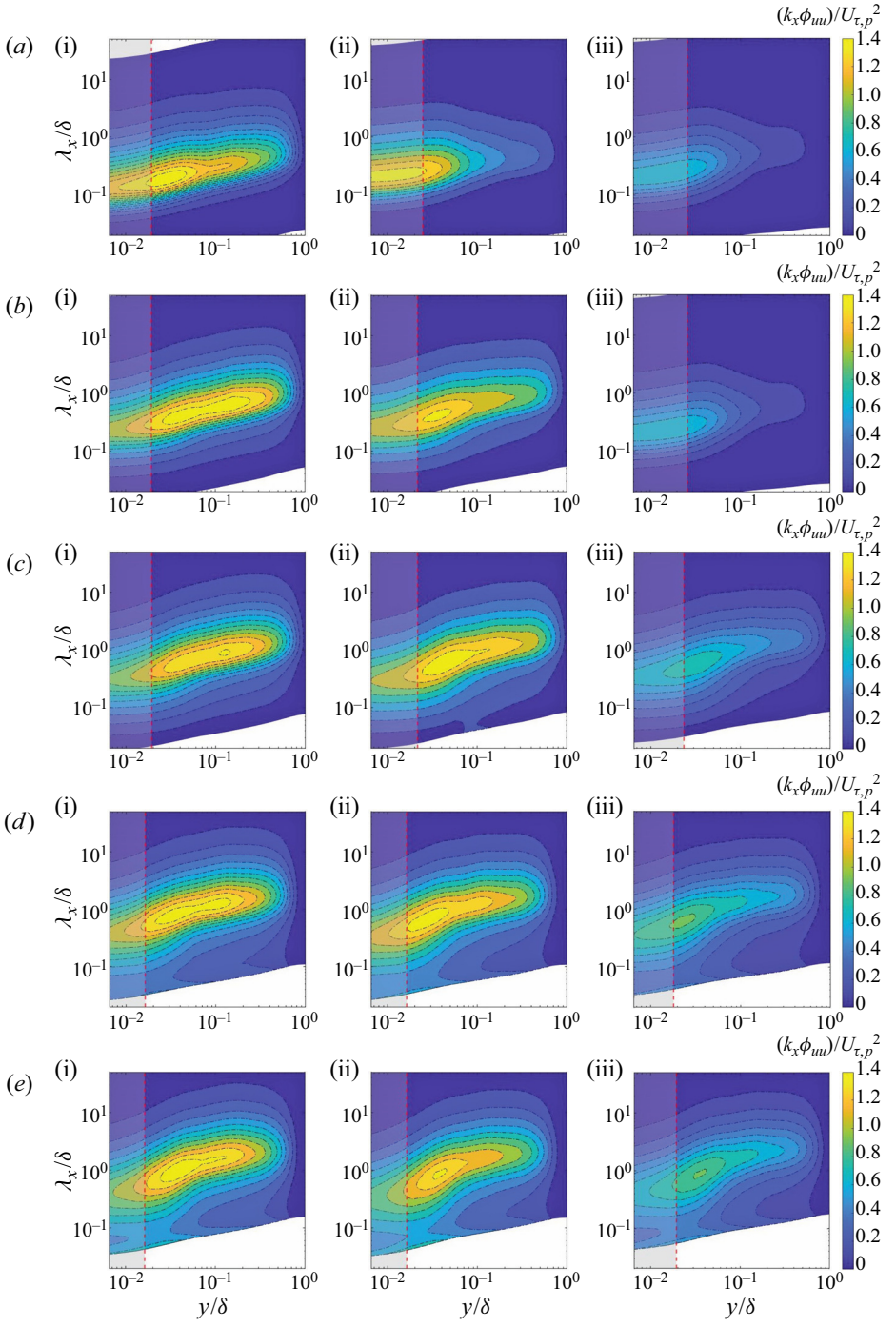

Figure 9. Two-dimensional spectrograms of the inner-normalised premultiplied velocity spectra ($k_x\phi_{uu}/U_{\tau,p}{}^2$) with (i) $U_s = 0$; (ii) $U_s = 1.45\ \mathrm{m\,s^{-1}}$; (iii) $U_s = 3.3\ \mathrm{m\,s^{-1}}$. The Re_τ is the lowest in (*a*) and highest in (*e*). The vertical dashed line corresponds to $y = k$.

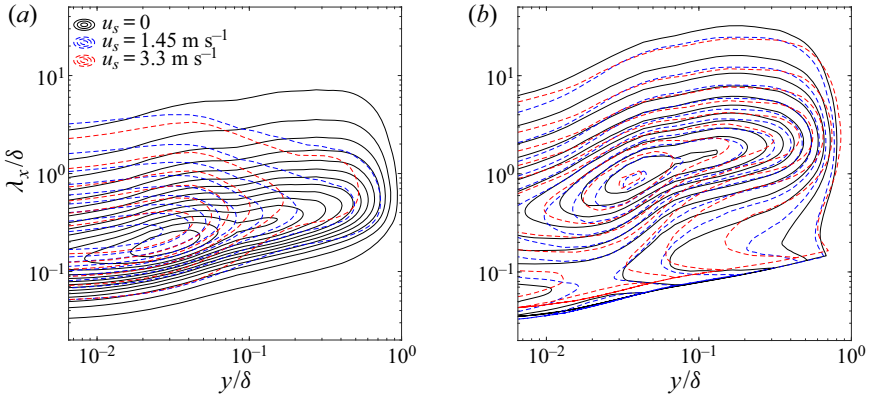

Figure 10. Comparison of contour lines of velocity spectra $(k_x\phi_{uu})/U_\tau^2$ at three suction velocities ($U_s = 0$, 1.45 and 3.3 m s^{-1}) for the lowest (*a*) and highest (*b*) Re_τ. Contour levels: 0–1.4 in 0.1 increments.

The contour maps (figure 9) for the two largest Reynolds numbers exhibit a behaviour on the lower end of λ_x across the boundary layer not observed in the contour maps for the lower Reynolds numbers. The contours indicate that the motions at low λ_x become relatively energetic, particularly in the region around $y = k$. At this stage one can speculate on the nature of the physical phenomenon responsible for this 'extra' energy. It is possible that the shear layers issued at the roughness elements become energetic enough to leave their imprint on the spectrograms. However, further investigation is required to comment conclusively.

3.5. *Comparison with smooth wall*

We have argued earlier that the response of the rough wall TBL to suction is different to that of a smooth wall due mainly to the difference in the mechanism for the energy production between the two TBLs. To ascertain this argument, we compare the effect of suction on the distributions of U, $\overline{u^2}$ and S_u between the two TBLs at approximately similar σ and Re_θ; the smooth wall data are extracted from Oyewola *et al.* (2003). Figure 11(*a*) shows the mean velocity profiles; also shown on that figure are the mean velocity profile for the undisturbed smooth wall TBL and the Blasius profile. When suction is applied on the smooth wall TBL, the distribution U^+ follows the Blasius profile up to $y^+ = 30$, revealing the relaminarisation trend impacted by the wall suction on the TBL. This relaminarisation trend reflects the presence of a local favourable pressure gradient induced by the wall suction. Further, as the TBL flows over the suction section, a good part of the inner layer is sucked out, thus disrupting dramatically the production generating process taking place near-the wall and a new inner layer starts to develop downstream of the suction strip. Flow visualisations (Djenidi *et al.* 2002) showed that downstream of the strip, suction stabilised the near-wall low-speed streaks by reducing their spanwise oscillations while maintaining them closer to the wall for a longer extent as compared with when there was no suction. This indicates that the new inner layer evolves in a laminar-like behaviour which is consistent with the relaminarisation trend shown on the velocity profile. This behaviour is well documented, for example in Antonia *et al.* (1995), Djenidi & Antonia (2001), Djenidi *et al.* (2002), Oyewola *et al.* (2003) and Djenidi, Agrawal & Antonia (2009). In the case of the rough wall TBL, where the viscous sublayer is practically absent, the turbulence production process is controlled by the roughness elements. Thus, while suction removes

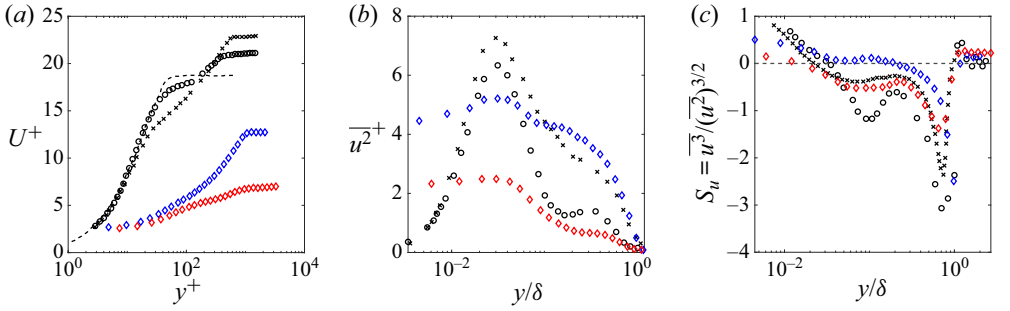

Figure 11. Comparison between the present data $U_s = 0$ (◇, blue), $U_s = 3.3$ m s^{-1} (i.e. σ = 3.4) (◇, red) at $Re_\theta = 2050$ and the smooth wall data of Oyewola *et al.* (2003) (Re_θ = 1400, (×) $\sigma = 0$, (◯) $\sigma = 3.3$). (*a*) Mean streamwise velocity (dashed line represents the Blasius profile, also extracted from Oyewola *et al.* (2003)), (*b*) turbulence intensity, (*c*) skewness (dashed line represents the magnitude of skewness in purely Gaussian signal).

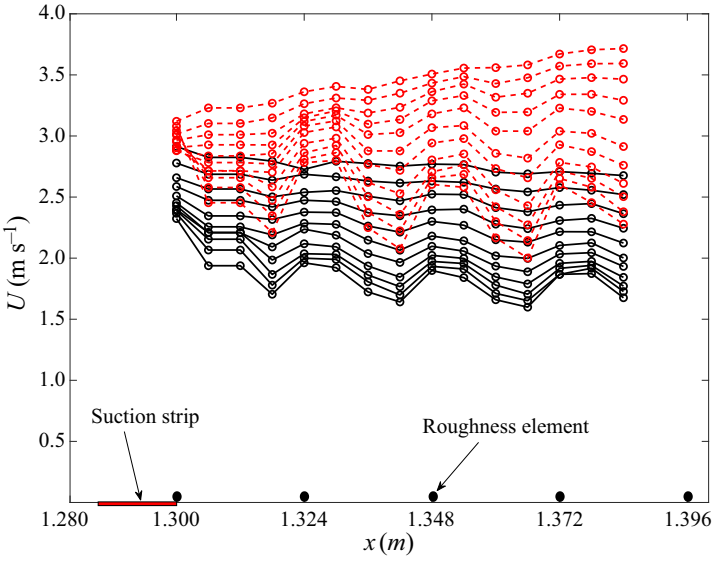

Figure 12. Streamwise variation of the mean velocity downstream of suction strip in the region $0.04 < y/\delta < 0.2$ (black lines, $U_s = 0$; dashed red lines, $U_s = 3.3$ m s^{-1}).

part of the inner layer of the incoming TBL, it does not modify the turbulence production mechanism and accordingly does not induce a relaminarisation trend, even though the TBL experiences a local favourable pressure gradient. Further, since the process of turbulence generation is unaffected or weakly affected, one can then expect that the memory effect to be weaker in the rough wall TBL than in the smooth wall TBL which is likely to lead to a shorter length recovery of the former TBL behind the suction strip.

Figure 11(*b*) shows the distribution of $\overline{u^2}^+$ for both rough and smooth wall TBLs with and without suction; note that the distributions are shown as a function of y/δ. Interestingly, while the mean velocity distribution for the smooth wall TBL with suction indicates relaminarisation, the distribution of $\overline{u^2}^+$ shows relatively high values of $\overline{u^2}^+$ in the region around $y/\delta = 0.03$ (or equivalently $y^+ = 13$). Remarkably, the location of the

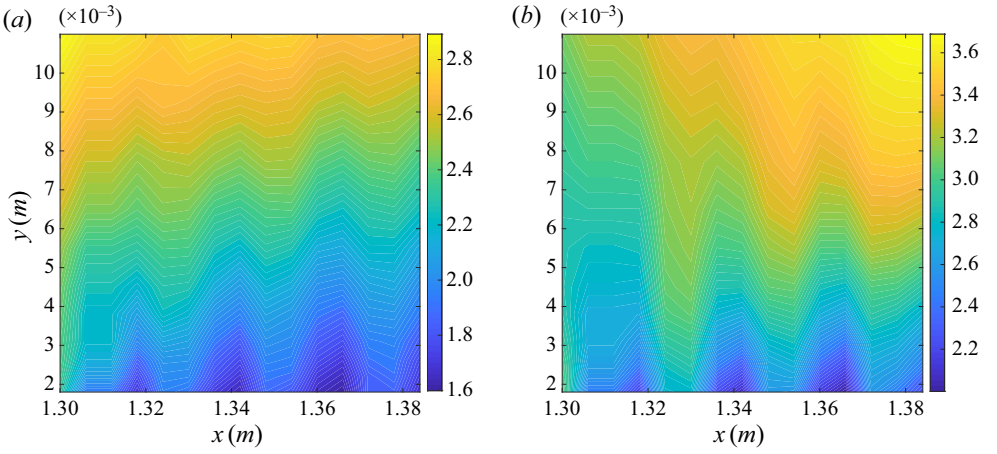

Figure 13. Isocontours of the streamwise mean velocity downstream of suction strip in the region $0.04 < y/\delta < 0.2$ for (*a*) $U_s = 0$ and (*b*) $U_s = 3.3\ \mathrm{m\,s^{-1}}$.

inner local peak of $\overline{u^2}^+$ in the smooth wall TBL remains unaffected by suction. This is also observed in the laser Doppler measurements of Djenidi *et al.* (2009) and the numerical results of Djenidi & Antonia (2001), but also in the measurements of Fernholz & Warnack (1998) and Warnack & Fernholz (1998) in a smooth wall TBL subjected to a favourable pressure gradient. In the case of wall suction, it is likely that the suction rate used was not strong enough to entirely destroy the turbulent energy production mechanism, thus leading to an incomplete relaminarisation. The magnitude of $\overline{u^2}^+$ in the region $0.1 \leq y/\delta \leq 1$ is reduced by suction. This is in agreement with the presence of a local favourable pressure gradient which has an effect of flattening the distribution of $\overline{u^2}^+$ in the outer region of the TBL as observed also in Fernholz & Warnack (1998) and Warnack & Fernholz (1998). This effect is also felt on the distribution of $\overline{u^2}^+$ in rough wall TBL when suction is applied.

Finally, we report in figure 11(*c*) the distributions of S_u for both TBLs with and without suction. In both TBLs, S_u decreases when suction is applied. However, S_u for the smooth wall TBL exhibits a stronger variation, in the form of an oscillation, than its rough wall counterpart within the region $0.07 \leq y/\delta \leq 0.2$. This certainly reflects a stronger structural change in the smooth wall TBL than in the rough wall TBL.

It was noted above that suction may not lead to a complete relaminarisation, which clearly warrants some attention. We thus carried out measurements over a streamwise distance up to $3\delta_0$ (where δ_0 is the initial boundary layer thickness at the leading edge of the suction strip) behind the suction strip. The results are reported in figure 12 which show the streamwise variation of the mean velocity over a vertical distance $0 < y/k < 7$. We used the lowest Reynolds number and highest suction rate since the boundary is most affected under these conditions. As expected, with no suction the velocity presents a periodic behaviour in the streamwise direction, which gradually vanishes as y/k increases. When suction is applied we can also observe the periodic behaviour and its disappearance with increasing y/k. However, there is a clear effect of suction. For a fixed y/k, the velocity increases. Notice the reverse trend between the no-suction and suction cases. For the former, the general trend is downward, while it is upward in the case of suction. This latter is caused by an inward rush of high-velocity flow caused by a downward flow deflection induced by suction. This trend difference is well captured in figure 13(*a*,*b*) which shows

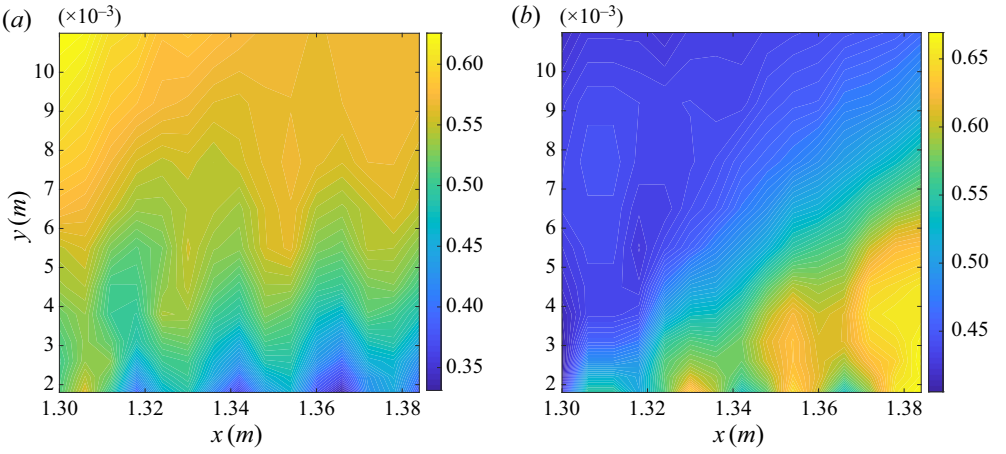

Figure 14. Isocontours of the streamwise velocity r.m.s. downstream of suction strip in the region $0.04 < y/\delta < 0.2$ for (*a*) $U_s = 0$ and (*b*) $U_s = 3.3\ \mathrm{m\,s^{-1}}$.

isocontours of the streamwise mean velocity. Each figure is almost the symmetric of the other. Figure 13(*a*) shows a general decrease in the velocity along x, while figure 13(*b*) shows an increase. The downward rush of high-velocity fluid also brings in the low turbulence intensity of the outer region of the flow as seen in figure 14. Interestingly, an increasing level of turbulence is observed (figure 14*b*) around the roughness elements with increasing x, reflecting an increasing turbulence activity in that region of the flow as the boundary layer starts its recovery. These results would confirm that relaminarisation cannot be achieved, or at least cannot be complete, in a rough wall TBL. Consequently, the downstream recovery distance of the TBL should be shorter on a rough wall than on a smooth wall.

4. Concluding remarks

The response of a ZPG rough wall TBL to a localised wall suction applied through a porous strip was investigated using hot-wire anemometry for various suction velocities and Reynolds numbers. The main results are as follows.

(i) The mean velocity profiles depart from the corresponding undisturbed profile for all Re_τ and suction velocities. The departure increases as the suction velocity, U_s, increases and $U_{\tau,p}$ decreases, although there is no relaminarisation trend of the TBL, as it can be observed in smooth wall TBL (Antonia *et al.* 1995; Oyewola *et al.* 2003).

(ii) Suction appears to increase the critical value of Re at which the TBL becomes a Re-independent. A parameter that controls this phenomenon is the ratio $U_s/U_{\tau,p}$. Unfortunately, the technical constraint of the experiment to increase/decrease this parameter over a wide range limits a full assessment of the effect of this parameter. It hoped that further studies where both $U_s/U_{\tau,p}$ and Re vary over several decades could be undertaken in the future.

(iii) The measurements show that suction reduces the longitudinal Reynolds stress across the boundary layer, regardless of the choice of the scaling variables.

(iv) Measurements of the longitudinal velocity skewness and flatness factor suggest possible structural changes in the boundary layer when suction is applied particularly at low Re.

(v) The two-dimensional contour maps of the velocity spectra revealed that suction reduces the energy at all scales of motion.

Altogether, these results indicate that the boundary layer response to suction is dependent of the ratio $U_s/U_{\tau,p}$, illustrating the critical role the combined effect of $U_{\tau,p}$ and U_s has on the control of the TBL: the larger $U_s/U_{\tau,p}$, the greater the effect of suction on the TBL. The results also show that as $U_s/U_{\tau,p}$ decreases, the TBL recovers an undisturbed state, whose initial conditions are controlled by the suction and its level of energy is lower than the undisturbed TBL. This is consistent with the following scenario: when suction is applied a new internal boundary layer develops downstream of the suction strip and grows outward into the existing boundary layer as it progresses downstream. This internal layer, which evolves on a rough wall, is structurally different from that evolving of a smooth wall subjected to the same wall suction. This is supported by a comparison between the effects of suction in rough wall and smooth wall TBLs. One can then expect to observe that the structural differences between these internal layers affect the TBL recovery downstream of the suction. For example, it is likely that the rough wall TBL recovers faster than the smooth wall TBL since the energy production must be bigger in the rough wall new internal layer than the smooth wall one. Also, the fact that the internal boundary layer evolves over a rough wall may prevent relaminarisation. This of course warrants further investigations.

Acknowledgements. The Authors wish to thank Dr K.M. Talluru (UNSW, Australia) for his assistance to post-process the data.

Funding. The authors gratefully acknowledge the support of the Australian Research Council, Discovery Project (ARC, DP190102751).

Declaration of interests. The authors report no conflict of interest.

Author ORCIDs.
F. Ghanadi https://orcid.org/0000-0002-6069-6105;
L. Djenidi https://orcid.org/0000-0001-8614-3595.

References

Abbassi, M.R., Baars, W.J., Hutchins, N. & Marusic, I. 2017 Skin-friction drag reduction in a high-Reynolds-number turbulent boundary layer via real-time control of large-scale structures. *Intl J. Heat Fluid Flow* **67**, 30–41.

Antonia, R.A., Fulachier, L., Krishnamoorthy, L.V., Benabid, T. & Anselmet, F. 1988 Influence of wall suction on the organized motion in a turbulent boundary layer. *J. Fluid Mech.* **190**, 217–240.

Antonia, R.A., Zhu, Y. & Sokolov, M. 1995 Effect of concentrated wall suction on a turbulent boundary layer. *Phys. Fluids* **7** (10), 2465–2474.

Bobke, A., Örlü, R. & Schlatter, P. 2016 Simulations of turbulent asymptotic suction boundary layers. *J. Turbul.* **17** (2), 157–180.

Chung, D. & McKeon, B.J. 2010 Large-eddy simulation of large-scale structures in long channel flow. *J. Fluid Mech.* **661**, 341–364.

Connelly, J.S., Schultz, M.P. & Flack, K.A. 2006 Velocity-defect scaling for turbulent boundary layers with a range of relative roughness. *Exp. Fluids* **40** (2), 188–195.

Çuhadaroğlu, B., Akansu, Y.E. & Turhal, A.O. 2007 An experimental study on the effects of uniform injection through one perforated surface of a square cylinder on some aerodynamic parameters. *Expl Therm. Fluid Sci.* **31** (8), 909–915.

Djenidi, L., Agrawal, A. & Antonia, R.A. 2009 Anisotropy measurements in the boundary layer over a flat plate with suction. *Expl Therm. Fluid Sci.* **33** (7), 1106–1111.

Djenidi, L. & Antonia, R.A. 2001 Calculation of the effect of concentrated wall suction on a turbulent boundary layer using a second-order moment closure. *Intl J. Heat Fluid Flow* **22** (5), 487–494.

DJENIDI, L., GALL, P.E., VINCENT, A. & ANTONIA, R.A. 2002 Effect of wall suction on the structure of a turbulent boundary layer. In *11th International Symposium on Applications of Laser Techniques in Fluid Mechanics. Paper No 23.1*.

DJENIDI, L., KAMRUZZAMAN, M. & DOSTAL, L. 2019*a* Effects of wall suction on a 2D rough wall turbulent boundary layer. *Exp. Fluids* **60** (3), 43.

DJENIDI, L., TALLURU, K.M. & ANTONIA, R.A. 2018 Can a turbulent boundary layer become independent of the Reynolds number? *J. Fluid Mech.* **851**, 1–22.

DJENIDI, L., TALLURU, K.M. & ANTONIA, R.A. 2019*b* A velocity defect chart method for estimating the friction velocity in turbulent boundary layers. *Fluid Dyn. Res.* **51** (4), 045502.

FERNHOLZ, H.H. & WARNACK, D. 1998 The effects of a favourable pressure gradient and of the Reynolds number on an incompressible axisymmetric turbulent boundary layer. Part 1. The turbulent boundary layer. *J. Fluid Mech.* **359**, 329–356.

GAD-EL HAK, M. & BLACKWELDER, R.F. 1989 Selective suction for controlling bursting events in a boundary layer. *AIAA J.* **27** (3), 308–314.

HEALZER, J., MOFFAT, R. & KAYS, W. 1974 The turbulent boundary layer on a porous, rough plate-experimentalheat transfer with uniform blowing. In *Thermophysics and Heat Transfer Conference*, p. 680.

HULTMARK, M., VALLIKIVI, M., BAILEY, S.C.C. & SMITS, A.J. 2013 Logarithmic scaling of turbulence in smooth-and rough-wall pipe flow. *J. Fluid Mech.* **728**, 376–395.

HUTCHINS, N., NICKELS, T.B., MARUSIC, I. & CHONG, M.S. 2009 Hot-wire spatial resolution issues in wall-bounded turbulence. *J. Fluid Mech.* **635**, 103–136.

JACKSON, P.S. 1981 On the displacement height in the logarithmic velocity profile. *J. Fluid Mech.* **111**, 15–25.

JACOBSON, S.A. & REYNOLDS, W.C. 1998 Active control of streamwise vortices and streaks in boundary layers. *J. Fluid Mech.* **360**, 179–211.

JOHANSSON, A.V. & ALFREDSSON, P.H. 1983 Effects of imperfect spatial resolution on measurements of wall-bounded turbulentbx shear flows. *J. Fluid Mech.* **137**, 409–421.

KAMETANI, Y., FUKAGATA, K., ÖRLÜ, R. & SCHLATTER, P. 2015 Effect of uniform blowing/suction in a turbulent boundary layer at moderate Reynolds number. *Intl J. Heat Fluid Flow* **55**, 132–142.

KAMRUZZAMAN, M., TALLURU, K.M., DJENIDI, L. & ANTONIA, R.A. 2014 An experimental study of turbulent boundary layer over 2d transverse circular bars. In *19th Australasian Fluid Mechanics Conference, Melbourne, Australia*.

KHAPKO, T., SCHLATTER, P., DUGUET, Y. & HENNINGSON, D.S. 2016 Turbulence collapse in a suction boundary layer. *J. Fluid Mech.* **795**, 356–379.

LEONARDI, S., ORLANDI, P., SMALLEY, R.J., DJENIDI, L. & ANTONIA, R.A. 2003 Direct numerical simulations of turbulent channel flow with transverse square bars on one wall. *J. Fluid Mech.* **491**, 229–238.

LIGRANI, P.M. & BRADSHAW, P. 1987 Spatial resolution and measurement of turbulence in the viscous sublayer using subminiature hot-wire probes. *Exp. Fluids* **5** (6), 407–417.

LOCKERBY, D.A., CARPENTER, P.W. & DAVIES, C. 2005 Control of sublayer streaks using microjet actuators. *AIAA J.* **43** (9), 1878–1886.

MARUSIC, I., TALLURU, K.M. & HUTCHINS, N. 2014 Controlling the large-scale motions in a turbulent boundary layer. In *Fluid-Structure-Sound Interactions and Control*, pp. 17–26. Springer.

MILLER, M.A., MARTIN, A. & BAILEY, S.C.C. 2014 Investigation of the scaling of roughness and blowing effects on turbulent channel flow. *Exp. Fluids* **55** (2), 1675.

MYOSE, R.Y. & BLACKWELDER, R.F. 1995 Control of streamwise vortices using selective suction. *AIAA J.* **33** (6), 1076–1080.

ÖRLÜ, R. & SCHLATTER, P. 2011 On the fluctuating wall-shear stress in zero pressure-gradient turbulent boundary layer flows. *Phys. Fluids* **23** (2), 021704.

OYEWOLA, O., DJENIDI, L. & ANTONIA, R.A. 2003 Combined influence of the Reynolds number and localised wall suction on a turbulent boundary layer. *Exp. Fluids* **35** (2), 199–206.

PARK, J. & CHOI, H. 1999 Effects of uniform blowing or suction from a spanwise slot on a turbulent boundary layer flow. *Phys. Fluids* **11** (10), 3095–3105.

QIAO, Z.X., ZHOU, Y. & WU, Z. 2017 Turbulent boundary layer under the control of different schemes. *Proc. R. Soc.* A **473** (2202), 20170038.

RATHNASINGHAM, R. & BREUER, K.S. 2003 Active control of turbulent boundary layers. *J. Fluid Mech.* **495**, 209–233.

REBBECK, H. & CHOI, K.-S. 2006 A wind-tunnel experiment on real-time opposition control of turbulence. *Phys. Fluids* **18** (3), 035103.

SCHETZ, J.A. & NERNEY, B. 1977 Turbulent boundary layer with injection and surface roughness. *AIAA J.* **15** (9), 1288–1294.

SEGAWA, T., MIZUNUMA, H., MURAKAMI, K., LI, F.-C. & YOSHIDA, H. 2007 Turbulent drag reduction by means of alternating suction and blowing jets. *Fluid Dyn. Res.* **39** (7), 552.

SQUIRE, D.T., HUTCHINS, N., MORRILL-WINTER, C., SCHULTZ, M.P., KLEWICKI, J.C. & MARUSIC, I. 2017 Applicability of Taylor's hypothesis in rough-and smooth-wall boundary layers. *J. Fluid Mech.* **812**, 398–417.

TALLURU, K.M., KULANDAIVELU, V., HUTCHINS, N. & MARUSIC, I. 2014 A calibration technique to correct sensor drift issues in hot-wire anemometry. *Meas. Sci. Technol.* **25** (10), 105304.

TAYLOR, G.I. 1938 The spectrum of turbulence. *Proc. R. Soc. Lond.* A **164** (919), 476–490.

TENNEKES, H., *et al.* 1972 *A First Course in Turbulence*. MIT Press.

WARNACK, D. & FERNHOLZ, H.H. 1998 The effects of a favourable pressure gradient and of the Reynolds number on an incompressible axisymmetric turbulent boundary layer. Part 2. The boundary layer with relaminarization. *J. Fluid Mech.* **359**, 357–381.

YOSHIOKA, S. & ALFREDSSON, P.H. 2006 Control of turbulent boundary layers by uniformwall suction and blowing. In *IUTAM Symposium on Laminar-Turbulent Transition*, pp. 437–442. Springer.